Sensor and Simulation Notes

Note 267

July 1980

Analytical Representation of ATLAS I (Trestle) Fields

F.C. Yang and K.S.H. Lee

The Dikewood Corporation
Santa Monica, California 90405

Abstract

Simple engineering analytical formulas are obtained for the ATLAS I fields. These formulas are derived by fitting the first TE surface wave of the ATLAS I wood platform to the field mapping data. An ad hoc term of the form $t\, e^{-\alpha t}$ is added to the analytical formulas to account for the "notch" in the ATLAS I field.

PREFACE

The authors would like to thank Drs. K.C. Chen and C.E. Baum of AFWL for helpful discussions, and O. Kaldirim and V. Tatoian of Dikewood for numerical computation.

CONTENTS

ILLUSTRATIONS

TABLES

I. INTRODUCTION

The results of past studies on bounded-wave simulator field environments in the working volume (Refs. 1 through 9) are strictly applicable to ALECS and ARES which do not have a wood stand. The wood stand (Figure 1) is an integral part of the ATLAS I (Trestle) and its presence will not only affect the field in the working volume, but also modify the responses of the test object. The former effect is deemed more significant than the latter. Numerical studies of the former effect have been accomplished in Reference 10. However, analytical studies are extremely invaluable to an overall understanding of the ATLAS I field environment in the working volume, and have never been conducted.

The objective of this report is to develop a simple electromagnetic model for the ATLAS I wood stand that will yield a simple engineering analytic form to describe accurately the ATLAS I field.

In Section II, formulas will be developed for the field distributions and dispersion relations of the TE surface-wave modes supported by dielectric layers. Section III is devoted to deriving numerical values appropriate for the ATLAS I simulator based on the formulas in Section II. In Section IV the numerical values will be compared with the ATLAS I field mapping data (Ref. 11) and simple engineering analytical formulas for the ATLAS I simulator fields will be obtained. Finally, in Section V a summary of important results will be given.

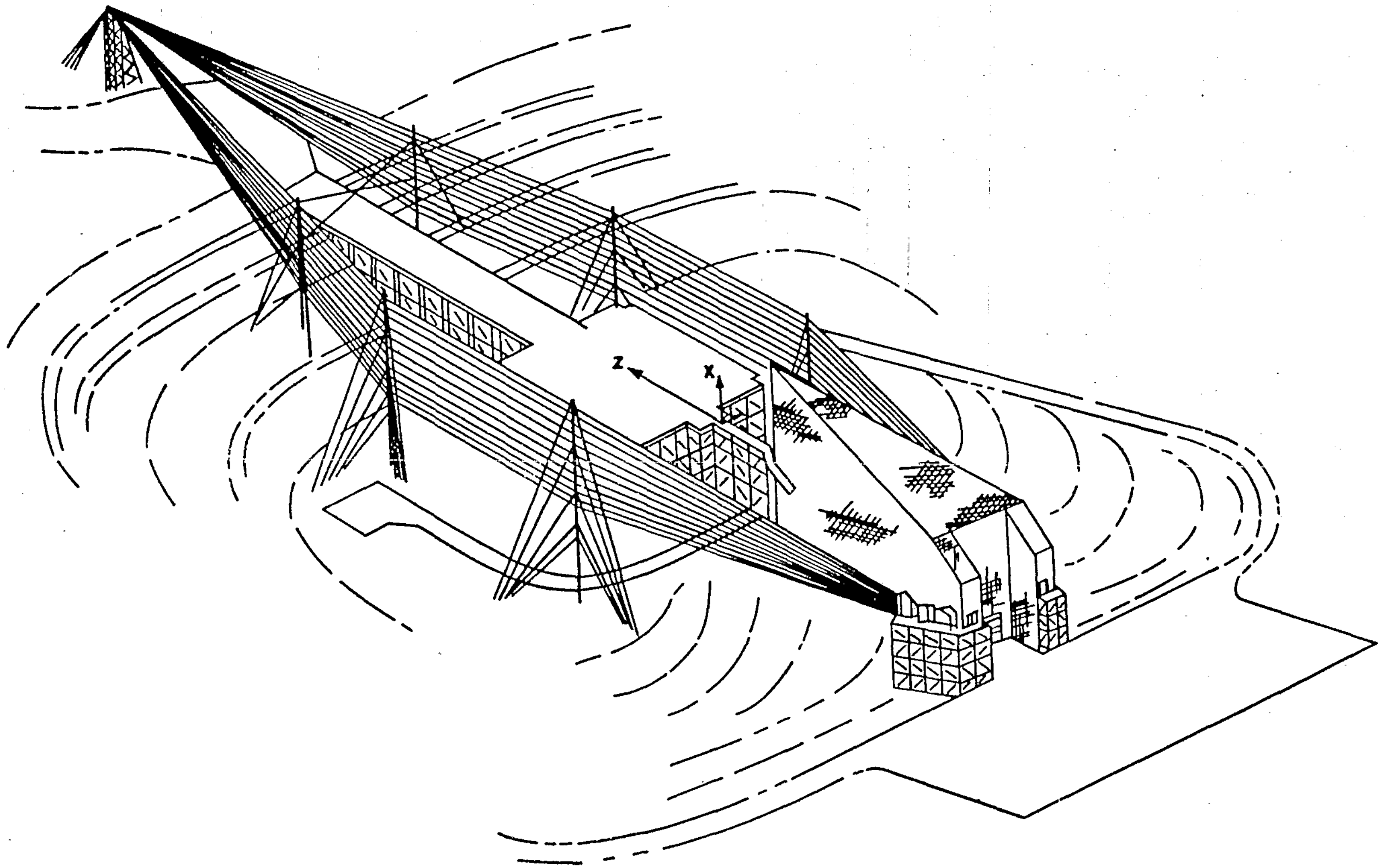

Figure 1. ATLAS I (Trestle) simulator with coordinate system indicated.

II. DISPERSION RELATION

Given a three-layered medium (Figure 2), the problem at hand is to find the propagation constant of the TE surface wave (H_x, H_z, E_y). The direction of propagation is along the z axis and there is no variation of the field in the y direction. The time variation of exp($j\omega t$) is assumed and suppressed.

To find the propagation constant one starts with Maxwell's equations

$$\nabla \times \vec{\tilde{E}} = -j\omega\mu\vec{\tilde{H}} \tag{1}$$

$$\nabla \times \vec{\tilde{H}} = j\omega\varepsilon\vec{\tilde{E}} \tag{2}$$

Since only $\tilde{E}_y$, $\tilde{H}_x$, $\tilde{H}_z$ are nonzero and $\partial/\partial y = 0$, then

$$\frac{\partial \tilde{E}_y}{\partial z} = j\omega\mu_o\tilde{H}_x \tag{3}$$

$$\frac{\partial \tilde{E}_y}{\partial x} = -j\omega\mu_o\tilde{H}_z \tag{4}$$

$$\frac{\partial \tilde{H}_z}{\partial x} - \frac{\partial \tilde{H}_x}{\partial z} = -j\omega\varepsilon\tilde{E}_y \tag{5}$$

from which one obtains

$$\left(\frac{d^2}{dx^2} + \omega^2\mu_o\varepsilon - \beta^2\right)\tilde{E}_y = 0 \tag{6}$$

where

$$\tilde{E}_y \propto e^{-j\beta z} \tag{7}$$

Equation 6 will be solved for each region shown in Figure 2.

1. Region 0 ($\varepsilon = \varepsilon_o$, $x \geq a/2$)

Assume there is no propagation in the x direction (decaying wave). The solution of Equation 6 for $\tilde{E}_y^{(0)}$ can be written in the following form:

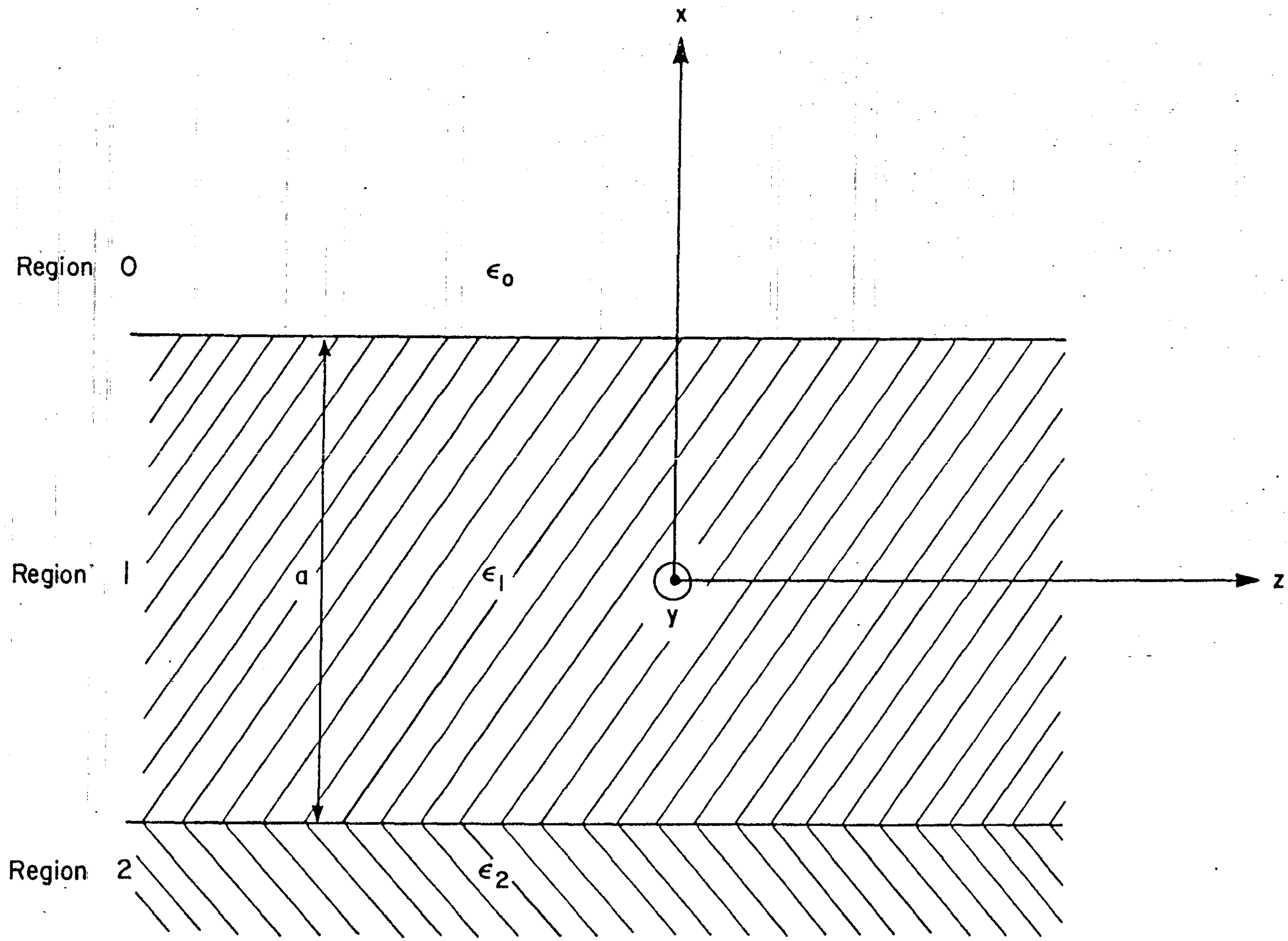

Figure 2. Basic configuration of the three-layered medium.

$$\tilde{E}_y^{(0)} = A\, e^{-\lambda_o x - j\beta z} \tag{8}$$

where

$$\lambda_o^2 = \beta^2 - k_o^2 = k_o^2\left(\xi^2 - 1\right) \tag{9}$$

$$k_o^2 = \omega^2 \mu_o \varepsilon_o, \qquad \xi^2 = \beta^2/k_o^2 \tag{10}$$

The other field components are

$$\tilde{H}_x^{(0)} = -\frac{\beta}{\omega\mu_o}\,\tilde{E}_y^{(0)} \tag{11}$$

$$\tilde{H}_z^{(0)} = -j\,\frac{\lambda_o}{\omega\mu_o}\,\tilde{E}_y^{(0)} \tag{12}$$

2. Region 1 ($\varepsilon_1 = \varepsilon_o \varepsilon_{1r}$, $-a/2 \leq x \leq a/2$)

Equation 6 takes the form

$$\left(\frac{d^2}{dx^2} + k_1^2 - \beta^2\right)\tilde{E}_y^{(1)} = 0 \tag{13}$$

the solution of which is given by

$$\tilde{E}_y^{(1)} = \left[B \sinh\left(\lambda_1 x\right) + C \cosh\left(\lambda_1 x\right)\right] e^{-j\beta z} \tag{14}$$

where

$$\lambda_1 = k_o\sqrt{\xi^2 - \varepsilon_{1r}}\,, \qquad k_1^2 = k_o^2 \varepsilon_{1r} \tag{15}$$

and

$$\tilde{H}_x^{(1)} = -\frac{\beta}{\omega\mu_o}\,\tilde{E}_y^{(1)} \tag{16}$$

$$\tilde{H}_z^{(1)} = -\frac{\lambda_1}{j\omega\mu_o}\left[B \cosh\left(\lambda_1 x\right) + C \sinh\left(\lambda_1 x\right)\right] e^{-j\beta z} \tag{17}$$

3. Region 2 ($\varepsilon_2 = \varepsilon_o \varepsilon_{2r}$, $x \le -a/2$)

Equation 6 is of the form

$$\left(\frac{d^2}{dx^2} + k_2^2 - \beta^2 \right) \tilde{E}_y^{(2)} = 0 \tag{18}$$

the solution of which with no propagation in the $-x$ direction is given by

$$\tilde{E}_y^{(2)} = D\, e^{\lambda_2 x - j\beta z} \tag{19}$$

where

$$\lambda_2 = k_o \sqrt{\xi^2 - \varepsilon_{2r}}\,, \qquad k_2^2 = k_o^2 \varepsilon_{2r} \tag{20}$$

and

$$\tilde{H}_x^{(2)} = -\frac{\beta}{\omega\mu_o} \tilde{E}_y^{(2)} \tag{21}$$

$$\tilde{H}_z^{(2)} = j \frac{\lambda_2}{\omega\mu_o} \tilde{E}_y^{(2)} \tag{22}$$

Matching the wave impedances across the interfaces one gets

$$\frac{\tilde{E}_y^{(0)}}{\tilde{H}_z^{(0)}} = \frac{\tilde{E}_y^{(1)}}{\tilde{H}_z^{(1)}} \quad \text{at} \quad x = \frac{a}{2} \tag{23}$$

$$\frac{\tilde{E}_y^{(1)}}{\tilde{H}_z^{(1)}} = \frac{\tilde{E}_y^{(2)}}{\tilde{H}_z^{(2)}} \quad \text{at} \quad x = -\frac{a}{2} \tag{24}$$

Substituting the field components given in Equations 8, 12, 14, 17, 19 and 22 into Equations 23 and 24 one obtains the dispersion relation

$$\tanh^2(\lambda_1 a/2) + 2\,\frac{\lambda_1^2 + \lambda_o\lambda_2}{\lambda_1(\lambda_2 + \lambda_o)} \tanh(\lambda_1 a/2) + 1 = 0 \tag{25}$$

which can be written in the following form

$$\tanh(\lambda_1 a) = \frac{-\lambda_1(\lambda_2 + \lambda_o)}{\lambda_1^2 + \lambda_o\lambda_2} \tag{26}$$

or

$$\tanh\left(k_o a\sqrt{\xi^2 - \varepsilon_{1r}}\right) = -\frac{\sqrt{\xi^2 - \varepsilon_{1r}}\left(\sqrt{\xi^2 - \varepsilon_{2r}} + \sqrt{\xi^2 - 1}\right)}{\left(\xi^2 - \varepsilon_{1r}\right) + \sqrt{\xi^2 - 1}\sqrt{\xi^2 - \varepsilon_{2r}}} \tag{27}$$

Equation 27 is the final form for the dispersion relation of the problem, and will be solved for ξ (= β/k_o) in the next section.

One could have defined $\lambda_1 = k_o\sqrt{\varepsilon_{1r} - \xi^2}$ in Equation 15 instead of $\lambda_1 = k_o\sqrt{\xi^2 - \varepsilon_{1r}}$. Then the hyperbolic functions sinh, cosh and tanh in Equations 14, 17, 25 and 26 could have become trigonometric functions sin, cos and tan after making the following replacements

$$\lambda_1 \rightarrow j\lambda_1$$
$$\sinh(\lambda_1 x) \rightarrow j\sin(\lambda_1 x)$$
$$\cosh(\lambda_1 x) \rightarrow \cos(\lambda_1 x)$$
$$\tanh(\lambda_1 x) \rightarrow j\tan(\lambda_1 x)$$

III. PROPAGATION CONSTANT AND WAVE IMPEDANCE

To find the normalized propagation constant ξ for given values of ε_{1r}, ε_{2r} and $k_o a$ one has to solve the dispersion Equation 27 numerically. Before presenting the numerical solution, the ranges of solution for real ξ under the condition of $\varepsilon_{1r} > \varepsilon_{2r} \geq 1$ are analyzed.

In the range where $\xi^2 \leq 1$, the left-hand side of Equation 27 is purely imaginary, but the right-hand side of this equation is real. This means that no roots are possible for $\xi^2 \leq 1$.

In the range where $\varepsilon_{2r} > \xi^2 > 1$, the left-hand side of Equation 27 is still purely imaginary but the right-hand side of this equation is complex. In order for this equation to have roots the real part of the right-hand side must be equal to zero. A little algebra shows that this is not possible. Thus, no roots exist within this range.

In the range where $\varepsilon_{1r} > \xi^2 \geq \varepsilon_{2r}$, both the left- and right-hand sides of Equation 27 are purely imaginary. This means that real roots for ξ may exist in this range.

In the range where $\xi^2 \geq \varepsilon_{1r}$, the right-hand side of Equation 27 is negative real and left-hand side is positive real. Hence, no roots are possible in this range.

The above simple analysis shows that the real normalized propagation constant ξ is limited to the range $\sqrt{\varepsilon_{1r}} > \xi \geq \sqrt{\varepsilon_{2r}}$. In the following, two cases will be considered, namely $\varepsilon_{2r} = 1.04$ and $\varepsilon_{2r} = 1$.

1. $\varepsilon_{2r} = 1.04$

From Reference 12, the dimensions and spacings of the wooden struts, the effective dielectric constant of the region below the wood platform is estimated to be about 1.04. Figure 3 shows ξ of the first TE surface-wave mode versus $k_o a$ for $\varepsilon_{2r} = 1.04$ and $\varepsilon_{1r} = 4,6,10$.

A closer look of Figure 3 and Equation 27 reveals that no real ξ, i.e., no propagation, is possible until some critical value of $k_o a$ is reached. Let this frequency be called the cutoff frequency of the surface wave.

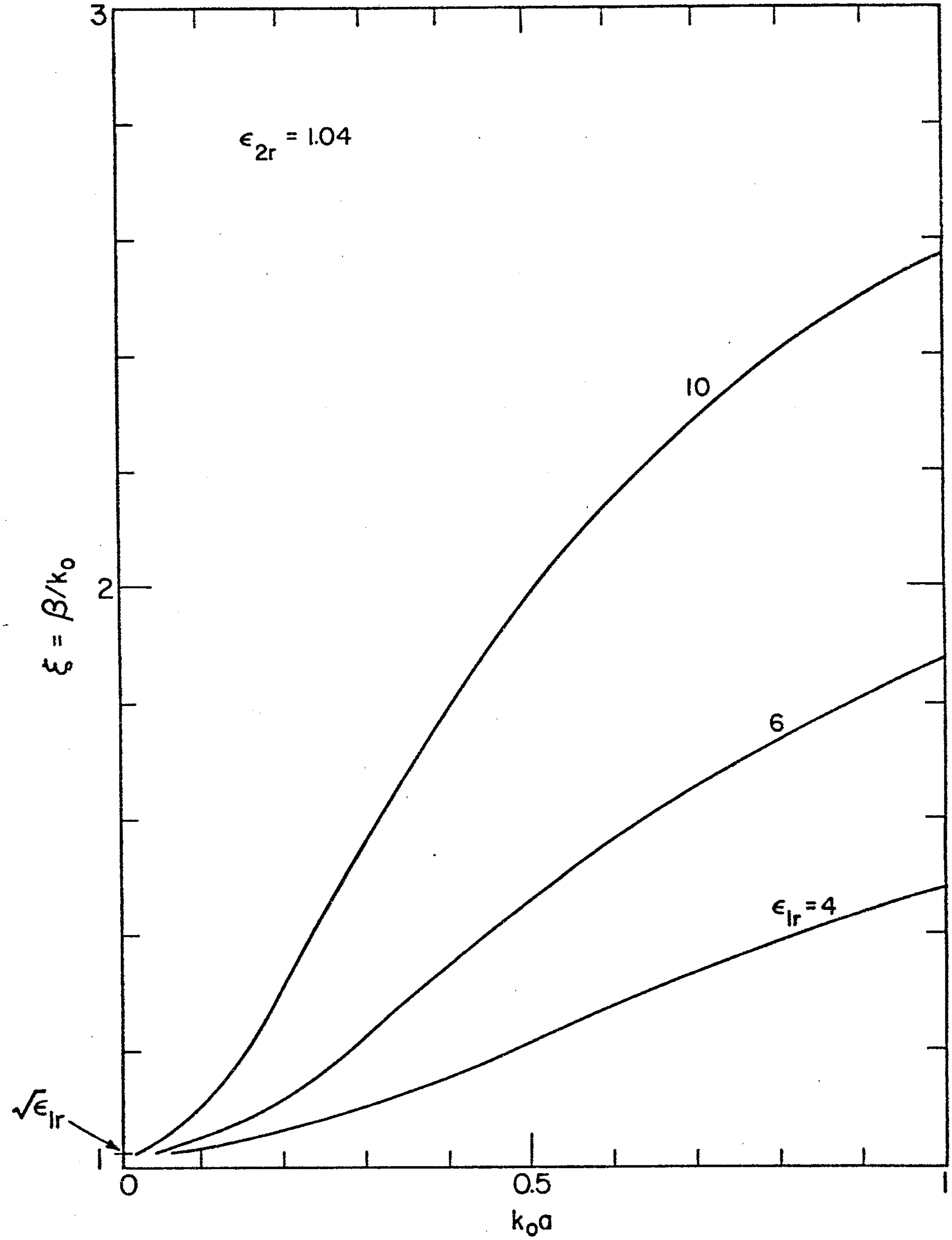

Figure 3. The normalized propagation constant ξ of the first TE surface-wave mode versus $k_o a$ for $\varepsilon_{2r} = 1.04$ and $\varepsilon_{1r} = 4,6,10$.

Obviously, the cutoff frequency can be obtained from Equation 27 with $\xi^2 = \varepsilon_{2r}$, that is,

$$\tanh\left(k_c^{(n)} a \sqrt{\varepsilon_{2r} - \varepsilon_{1r}}\right) = \frac{\sqrt{\varepsilon_{2r} - \varepsilon_{1r}}\sqrt{\varepsilon_{2r} - 1}}{\varepsilon_{1r} - \varepsilon_{2r}}$$

which gives

$$f_c^{(n)} = \frac{(n-1)\pi + \arctan\left(\sqrt{(\varepsilon_{2r} - 1)/(\varepsilon_{1r} - \varepsilon_{2r})}\right)}{2\pi a\sqrt{\varepsilon_{1r} - \varepsilon_{2r}}} \times 3 \times 10^8$$

Here, $f_c^{(n)}$ is the cutoff frequency of the nth mode of the surface wave. The first three cutoff frequencies are given in Table 1.

TABLE 1. FIRST THREE CUTOFF FREQUENCIES

n	ε_{1r}	ε_{2r}	a(m)	$f_c^{(n)}$ (MHz)	$k_c^{(n)} a$
1	4	1.04	1	3.2	0.0673
2	4	1.04	1	90.4	1.8933
3	4	1.04	1	177.6	3.7193

Figure 4 shows the normalized cutoff frequency $(k_c^{(1)} a)$ versus ε_{2r} for $\varepsilon_{1r} = 4$–10.

2. $\varepsilon_{2r} = 1$

When $\varepsilon_{2r} = 1$, Equation 27 becomes, for modes with $\tilde{H}_x(-x) = \tilde{H}_x(x)$,

$$\tanh\left(k_o a\sqrt{\xi^2 - \varepsilon_{1r}}\ /2\right) = -\frac{\sqrt{\xi^2 - 1}}{\sqrt{\xi^2 - \varepsilon_{1r}}} \tag{28}$$

and becomes, for modes with $\tilde{H}_x(-x) = -\tilde{H}_x(x)$

$$\coth\left(k_o a\sqrt{\xi^2 - \varepsilon_{1r}}/2\right) = -\frac{\sqrt{\xi^2 - 1}}{\sqrt{\xi^2 - \varepsilon_{1r}}}$$

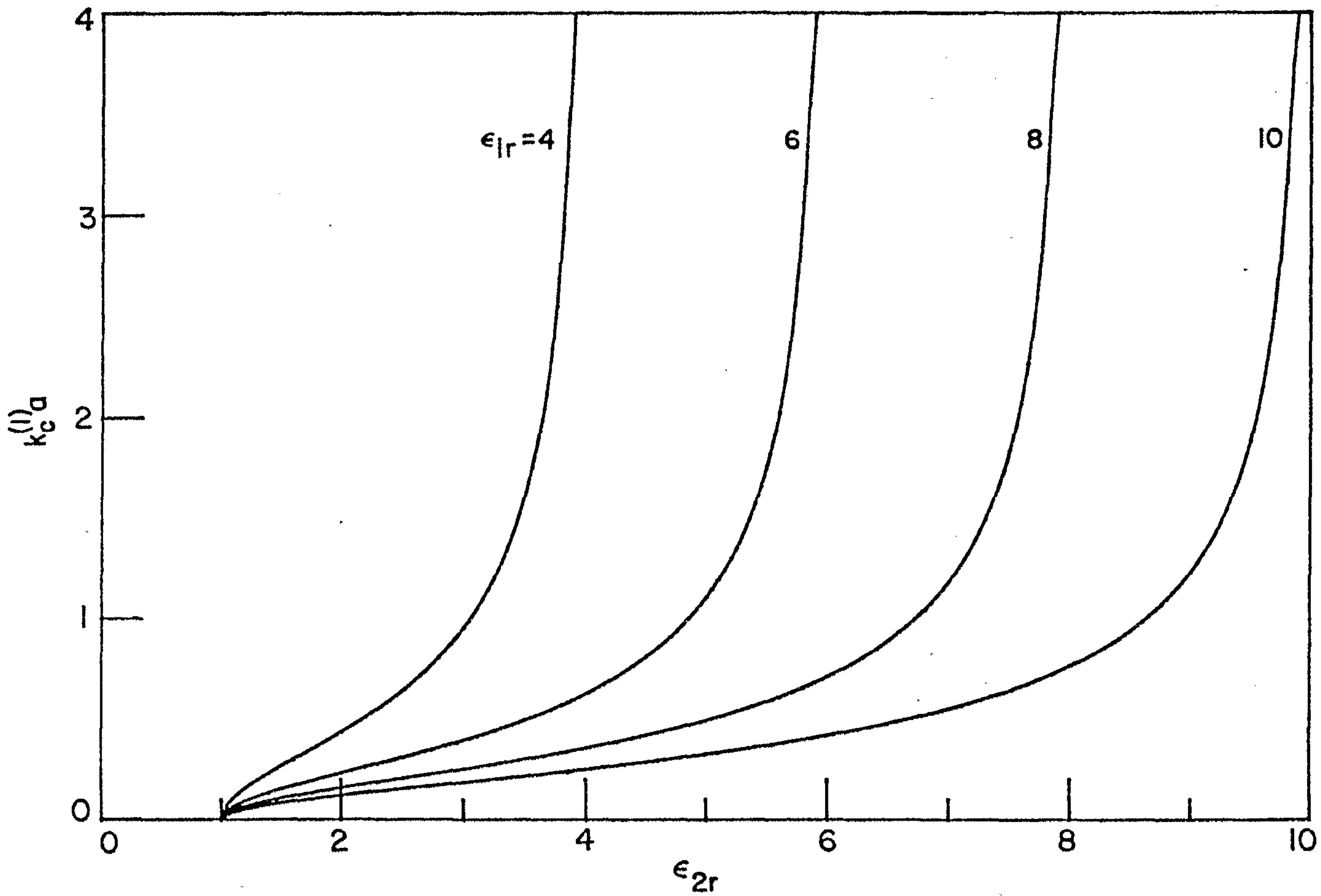

Figure 4. The cutoff frequency $k_c^{(1)}a$ of the first TE surface-wave mode versus ε_{2r} for $\varepsilon_{1r} = 4,6,8,10$.

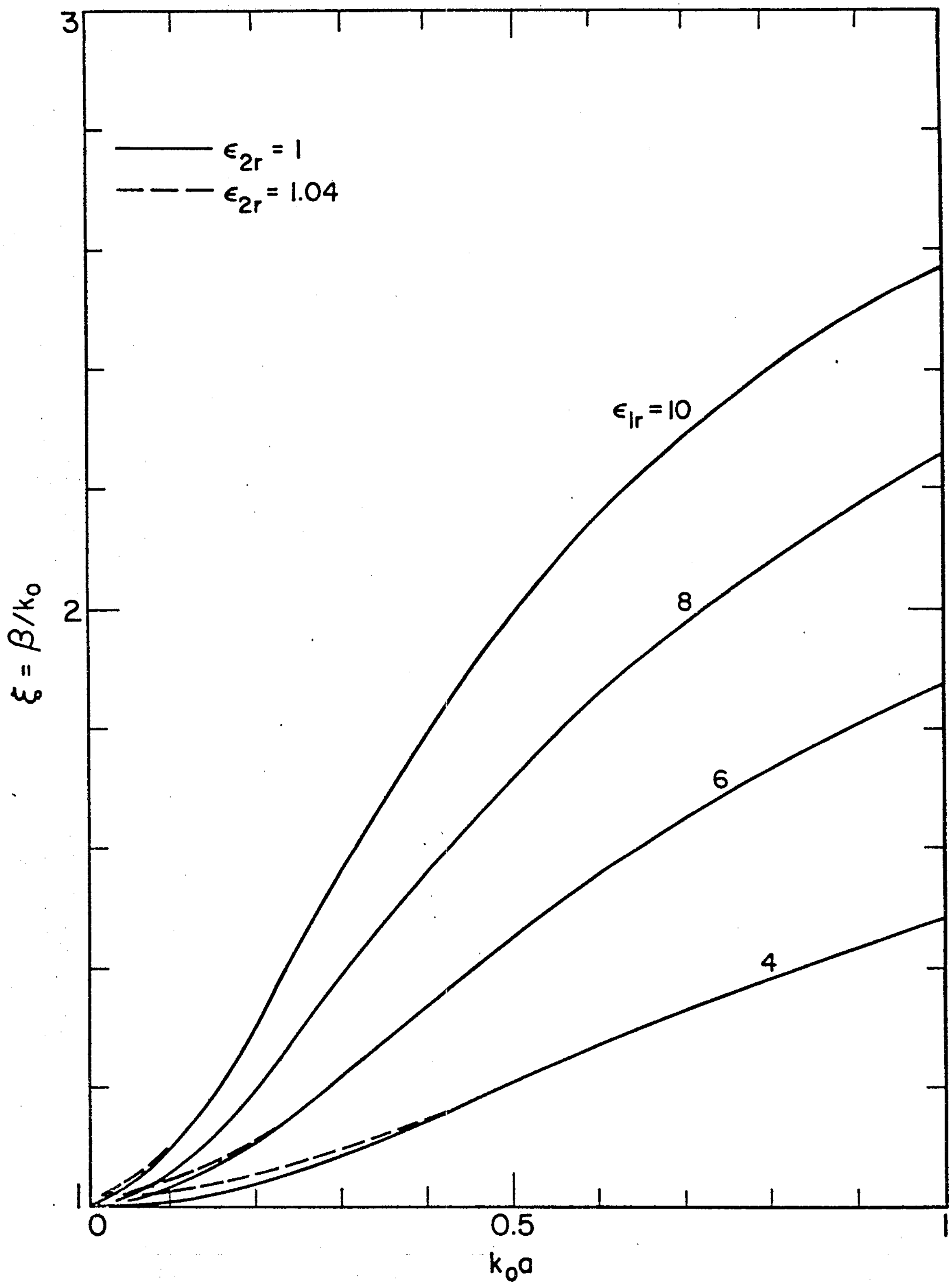

Figure 5. The normalized $\xi = \beta/k_o$ of the first TE surface-wave mode versus $k_o a$ for $\epsilon_{2r} = 1$, 1.04 and $\epsilon_{1r} = 4,6,8,10$.

The normalized propagation constant ξ has real values under the condition $\varepsilon_{1r} > 1$ at any frequency. Figure 5 shows ξ of the first TE surface-wave mode versus $k_o a$ for various ε_{1r}. It clearly shows that there is no cutoff frequency for $\varepsilon_{2r} = 1$.

In Figure 5, the ξ-value versus $k_o a$ for $\varepsilon_{2r} = 1.04$ is also given. It is observed that the difference in ξ-values for $\varepsilon_{2r} = 1$ and $\varepsilon_{2r} = 1.04$ is generally negligible except at very small $k_o a$. Thus, only the simpler results with $\varepsilon_{2r} = 1$ will be used in the following discussion and for the comparison with the field mapping data.*

After obtaining ξ, the impedances $\tilde{E}_y^{(0)}/\tilde{H}_z^{(0)}$ and $\tilde{E}_y^{(0)}/\tilde{H}_x^{(0)}$ can be calculated from the following two equations:

$$\frac{\tilde{E}_y^{(0)}}{\tilde{H}_z^{(0)}} = -j \frac{\omega\mu_o}{k_o\sqrt{\xi^2 - 1}} = -j \frac{Z_o}{\sqrt{\xi^2 - 1}} \tag{29}$$

$$\frac{\tilde{E}_y^{(0)}}{\tilde{H}_x^{(0)}} = -\frac{\omega\mu_o}{\beta} = -\frac{Z_o}{\beta/k_o} = -\frac{Z_o}{\xi} \tag{30}$$

which are plotted in Figures 6 and 7 for $\varepsilon_{2r} = 1$ and various ε_{1r}.

In the next section, the above results will be used to compare with the ATLAS I field mapping data.

*Since Table 1 shows that the first cutoff frequency is about 3.2 MHz for $\varepsilon_{1r} = 4$ and $\varepsilon_{2r} = 1.04$, one may question the validity of neglecting the lower medium with $\varepsilon_{2r} = 1.04$. However, at this frequency, the effect of the ground is no longer negligible. When the ground is properly taken into account, there will be no cutoff phenomenon.

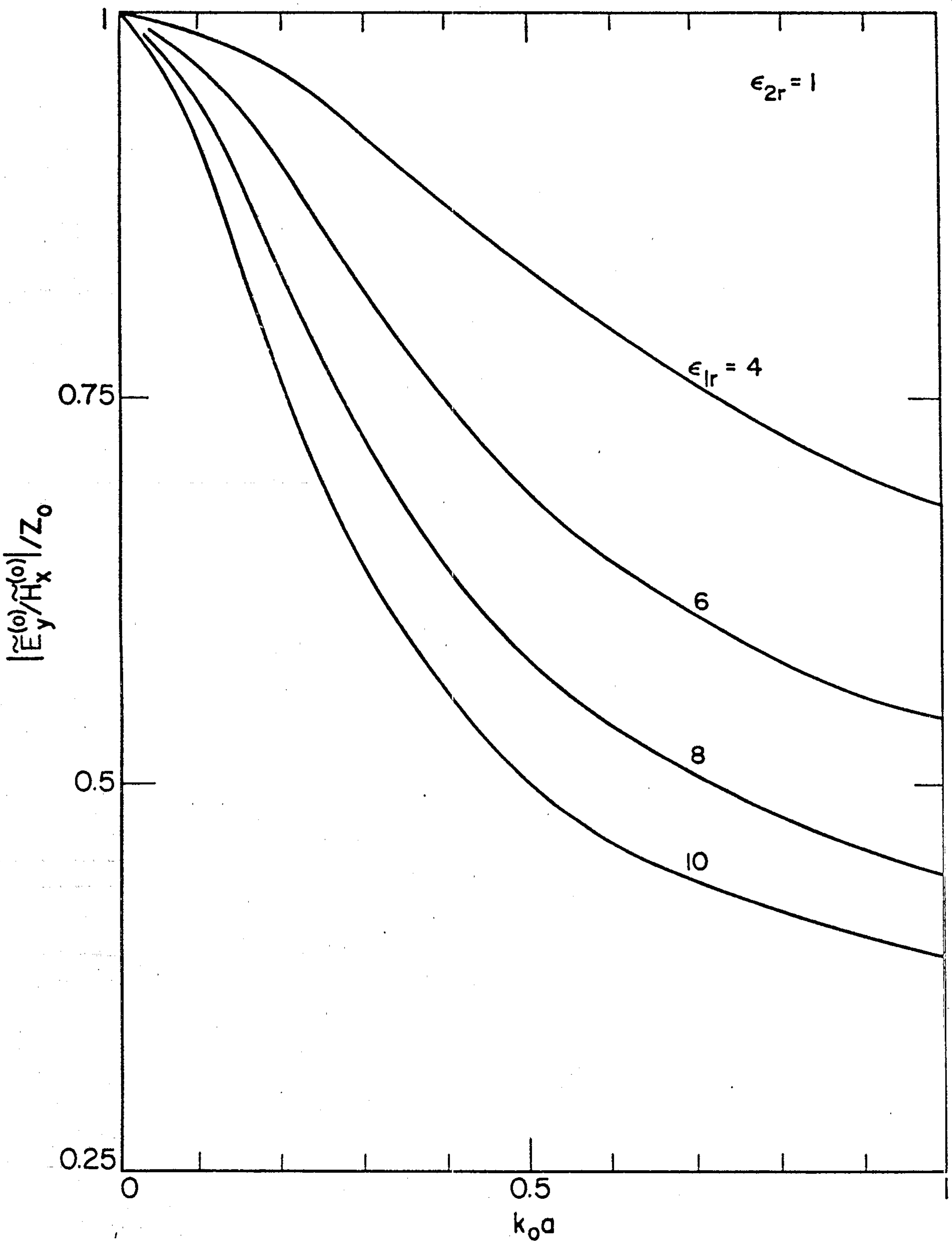

Figure 6. Normalized $|\tilde{E}_y^{(0)}/\tilde{H}_x^{(0)}|$ of the first TE surface-wave mode versus $k_o a$ for $\varepsilon_{2r} = 1$ and $\varepsilon_{1r} = 4,6,8,10$.

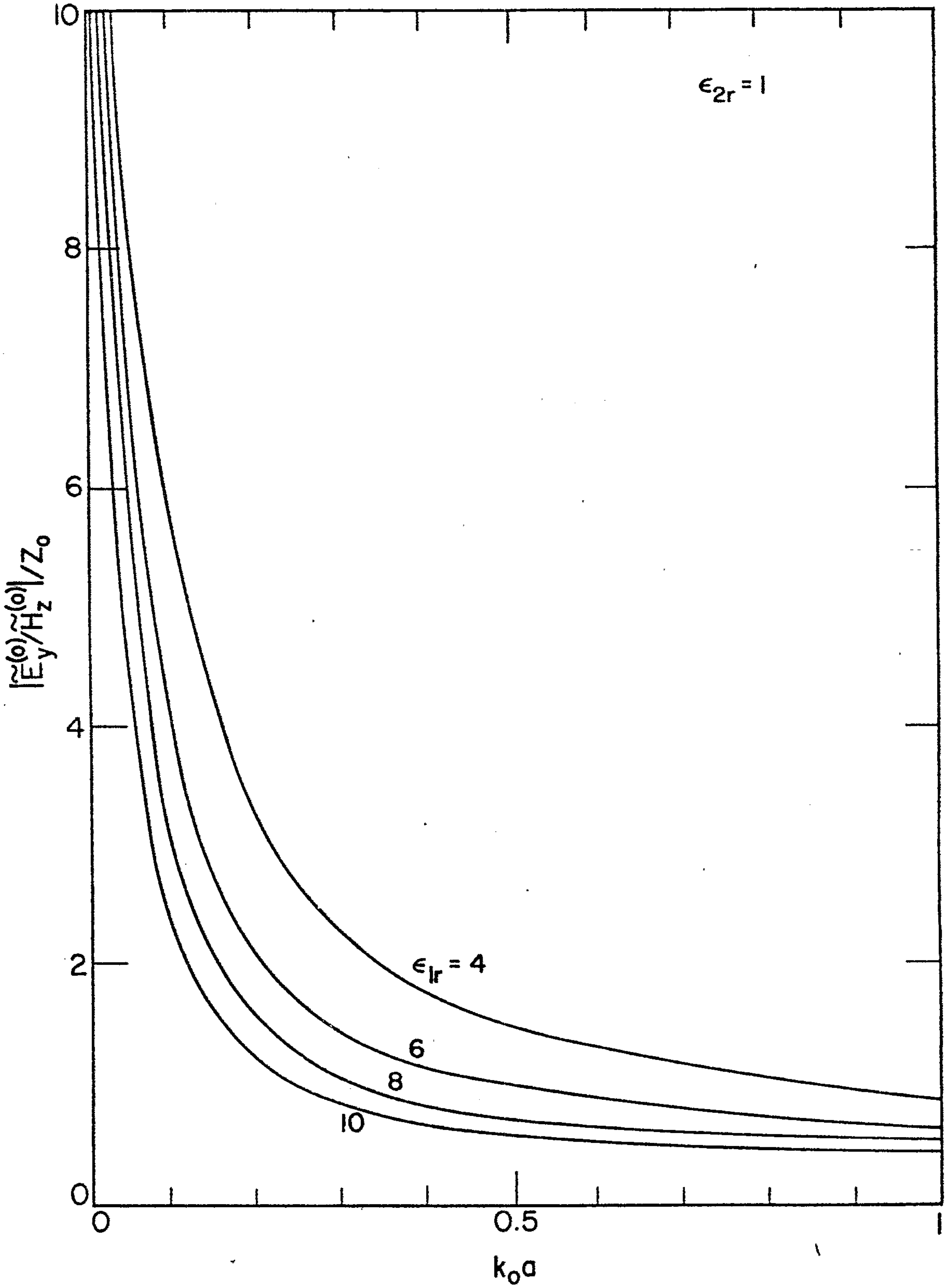

Figure 7. Normalized $|\tilde{E}_y^{(0)}/\tilde{H}_z^{(0)}|$ of the first TE surface-wave mode versus $k_o a$ for $\varepsilon_{2r} = 1$ and $\varepsilon_{1r} = 4,6,8,10$.

IV. ANALYTICAL REPRESENTATION OF ATLAS I FIELDS

In this section, the first TE surface-wave mode described in the previous sections will be used to represent the field distributions within the ATLAS I simulator.

In Section III, curves for the ratio of the electric to magnetic field (i.e., the wave impedances) of the first TE surface wave versus frequency were obtained. The impedance curves (without normalization) for $\varepsilon_{1r} = 4$, 10, and a = 0.5, 1, 1.5m are plotted in Figures 8 and 9 in the log-log scale. In the figures, the impedances deduced from the ATLAS I field mapping data (Ref. 11) are also given. Good agreements are observed between the field mapping data and the analytical results based on the first TE surface-wave mode when $\varepsilon_{1r} \simeq 4$ and $a \simeq 1$. (Also, see the final remark on pages 29 and 30).

In Figures 8 and 9, all the available field mapping data have been used to obtain the impedances except for test points 17 and 21 whose impedances are expected to be approximately equal to those of test points 13 and 22 (Figure 10). Figure 10 shows all the test points that are in Reference 11.

The good agreement shown in Figures 8 and 9 gives one the confidence in using the first TE surface-wave mode for describing the ATLAS I fields. The next step is the determination of the constant A in Equation 8. To this end, the field mapping data of test point 2 are used. One typical set of the frequency-domain curves of $\tilde{E}_y^{(0)}$ and $\tilde{H}_x^{(0)}$ at this test point is given in Figure 11. The frequency dependences of $\tilde{E}_y^{(0)}$ and $\tilde{H}_x^{(0)}$ are almost the same, as they should be according to Equation 11, for the frequency range where $k_o a \lesssim 0.2$ (frequency $\lesssim$ 10 MHz). The asymptotes are drawn in Figure 11 in broken lines leading to the following form for the constant A:

$$A = \frac{Z_o \tilde{H}_o}{(1 + st_1)(1 + st_2)} \tag{31}$$

where

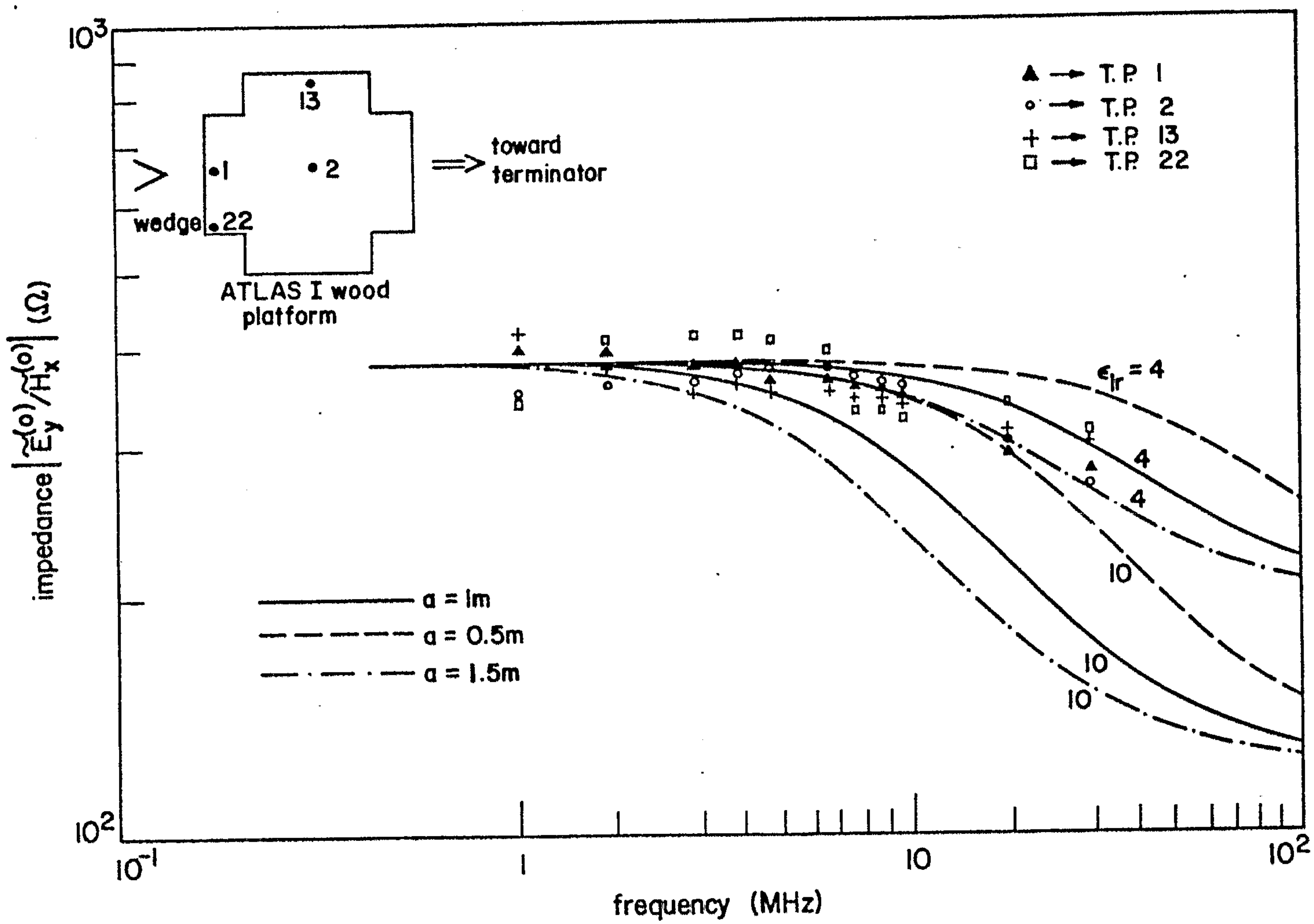

Figure 8. Wave impedance $|\tilde{E}_y^{(0)}/\tilde{H}_x^{(0)}|$ of the first TE surface-wave mode and those deduced from the ATLAS I field mapping data (Ref. 11).

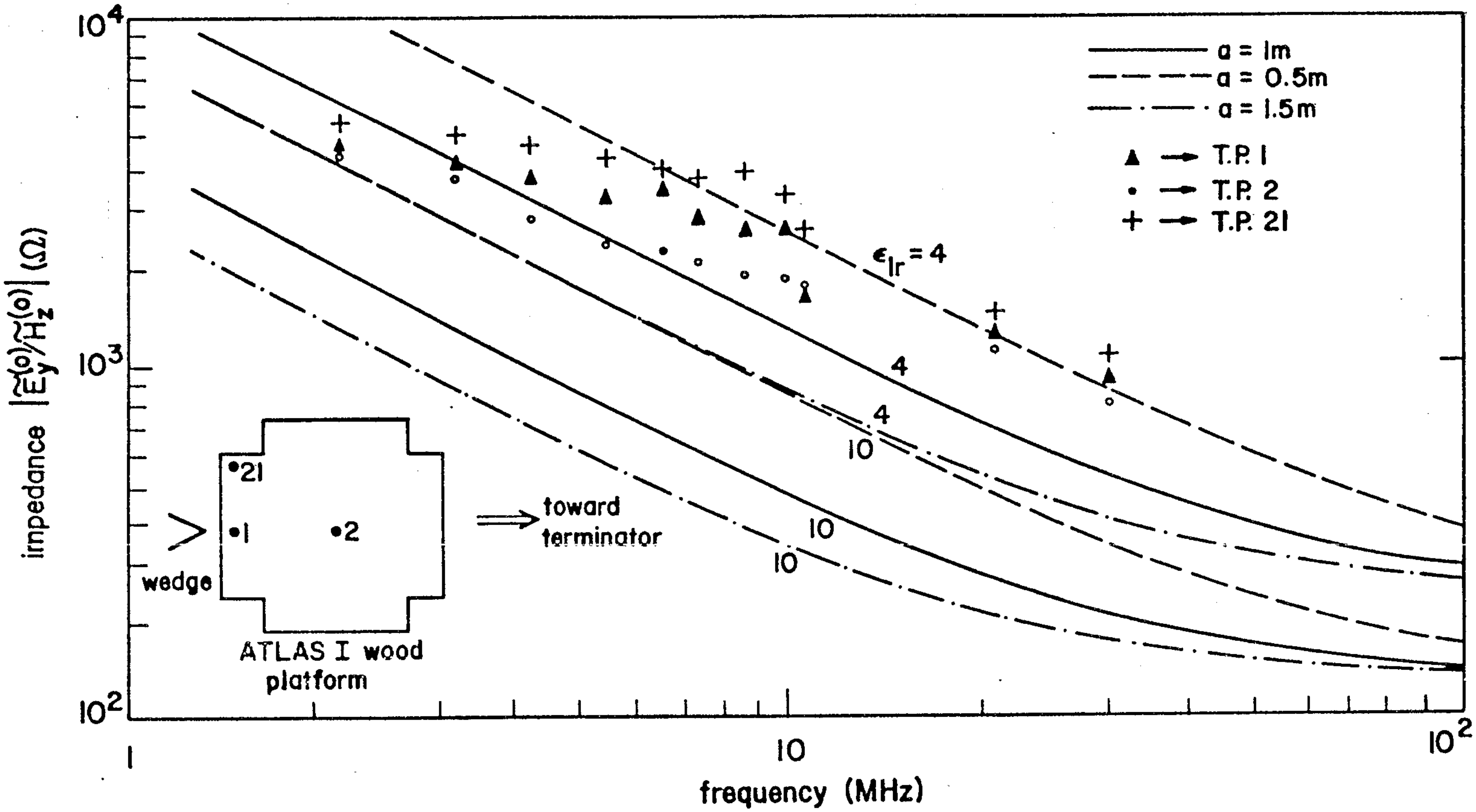

Figure 9. Wave impedance $|\tilde{E}_y^{(0)}/\tilde{H}_z^{(0)}|$ of the first TE surface-wave mode and those deduced from the ATLAS I field mapping data (Ref. 11).

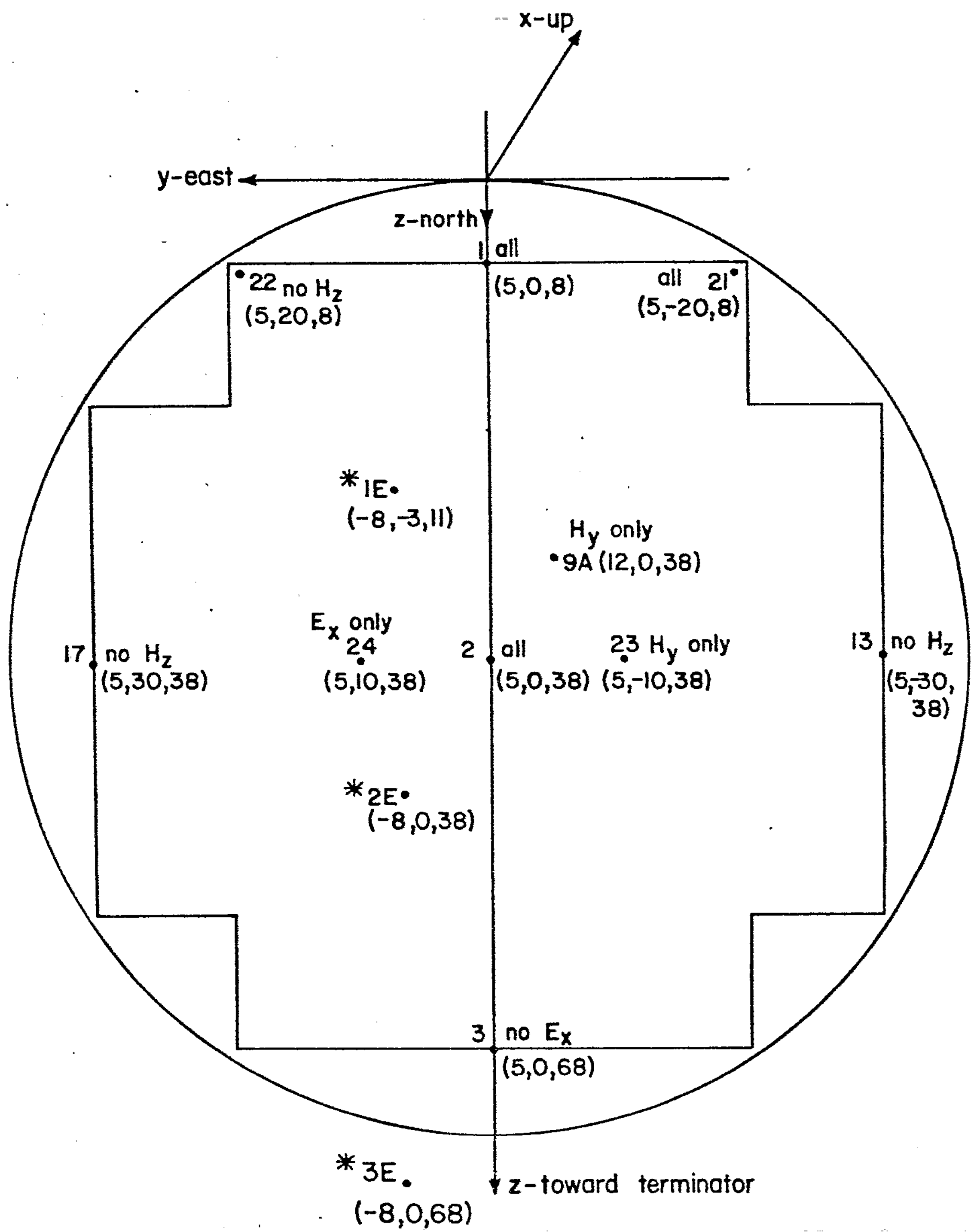

* Test points where only time-domain peak values were given.

Figure 10. Test points for which ATLAS I field mapping data are given in Reference 11.

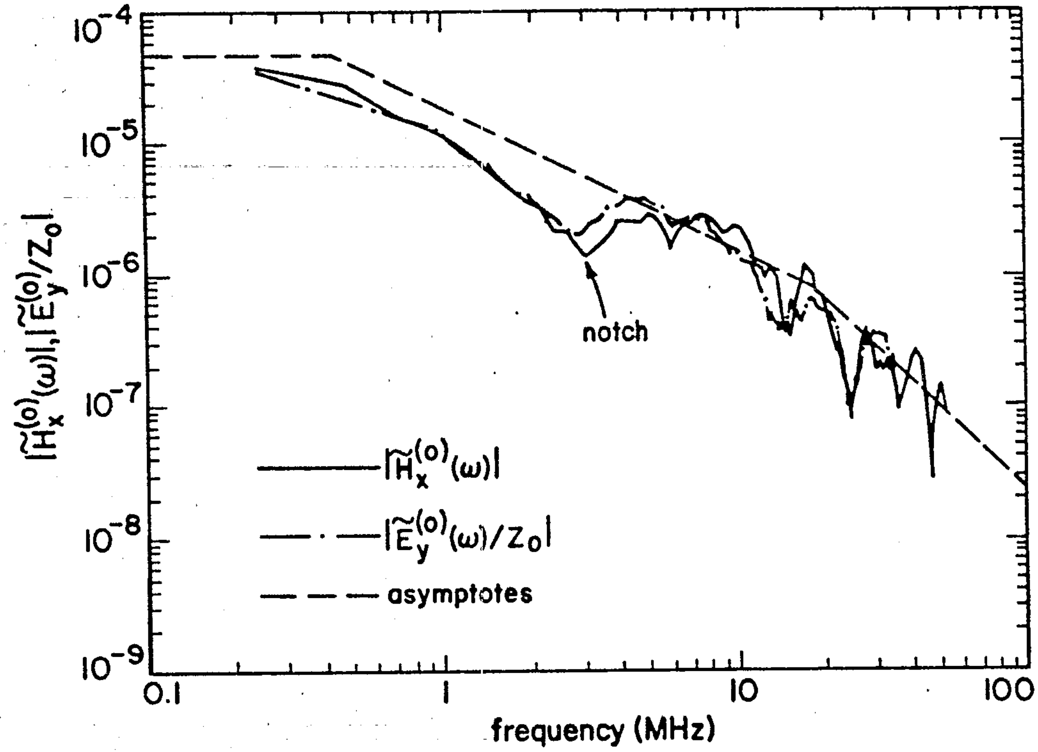

Figure 11. Frequency-domain curves of measured $\tilde{E}_y^{(0)}$ and $\tilde{H}_x^{(0)}$ at test point 2 and their asymptotes (Ref. 11).

$$\tilde{H}_o = 6 \times 10^{-5} \text{Amp}/(\text{m-Hz})$$

$$t_1 = 3 \times 10^{-7} \text{sec}$$

$$t_2 = 8 \times 10^{-9} \text{sec}$$

In obtaining Equation 31, one has assumed $\lambda_o x \approx 0$ at test point 2, and ignored the "notch" effect.

From Equations 8, 11 and 31, the time-domain $E_y^{(0)}(t)$ and $H_x^{(0)}(t)$ at test point 2 are

$$H_x^{(0)}(t) = -E_y^{(0)}(t)/Z_o = -\frac{\tilde{H}_o}{t_1 - t_2}\left(e^{-t/t_1} - e^{-t/t_2}\right) \tag{32}$$

which is plotted in Figure 12. The agreement with field mapping data at late times is very excellent. But there is considerable difference at early times. The difference is attributable to the notch existing in the pulser voltages. To account for the notch effect, one may subtract a term from Equation 32. From Figure 11 one can see that in the frequency domain the term to be subtracted should behave as $|1/s^2|$ when $|s|$ is large, and should have a double pole at $\simeq$ 3 MHz. Such a term has a time variation of the form $t \exp(-t/t_o)$ with $t_o = 6 \times 10^{-8}$sec. Thus, one has

$$H_x^{(0)}(t) = -E_y^{(0)}(t)/Z_o = -\frac{\tilde{H}_o}{t_1 - t_2}\left(e^{-t/t_1} - e^{-t/t_2} - \frac{1.8t}{t_o} e^{-t/t_o}\right) \tag{33}$$

where the coefficient $1.8/t_o$ is chosen in such a way that the best agreement between Equation 33 and the field mapping curve can be obtained (except for the pre-pulse region, see Figure 12).

From Equations 12 and 33 the z-component of the ATLAS I magnetic field can also be estimated. Generally, it will involve solving Equations 28 and 9 to obtain λ_o as a function of ω and subsequently inverting complicated Fourier (or Laplace) integral. However, if one is only interested in the late-time behavior of $H_z^{(0)}(t)$ where the high-frequency part of the spectrum is not important, a simple expression for $H_z^{(0)}(t)$ can be obtained in the following manner: From Equation 12, one has

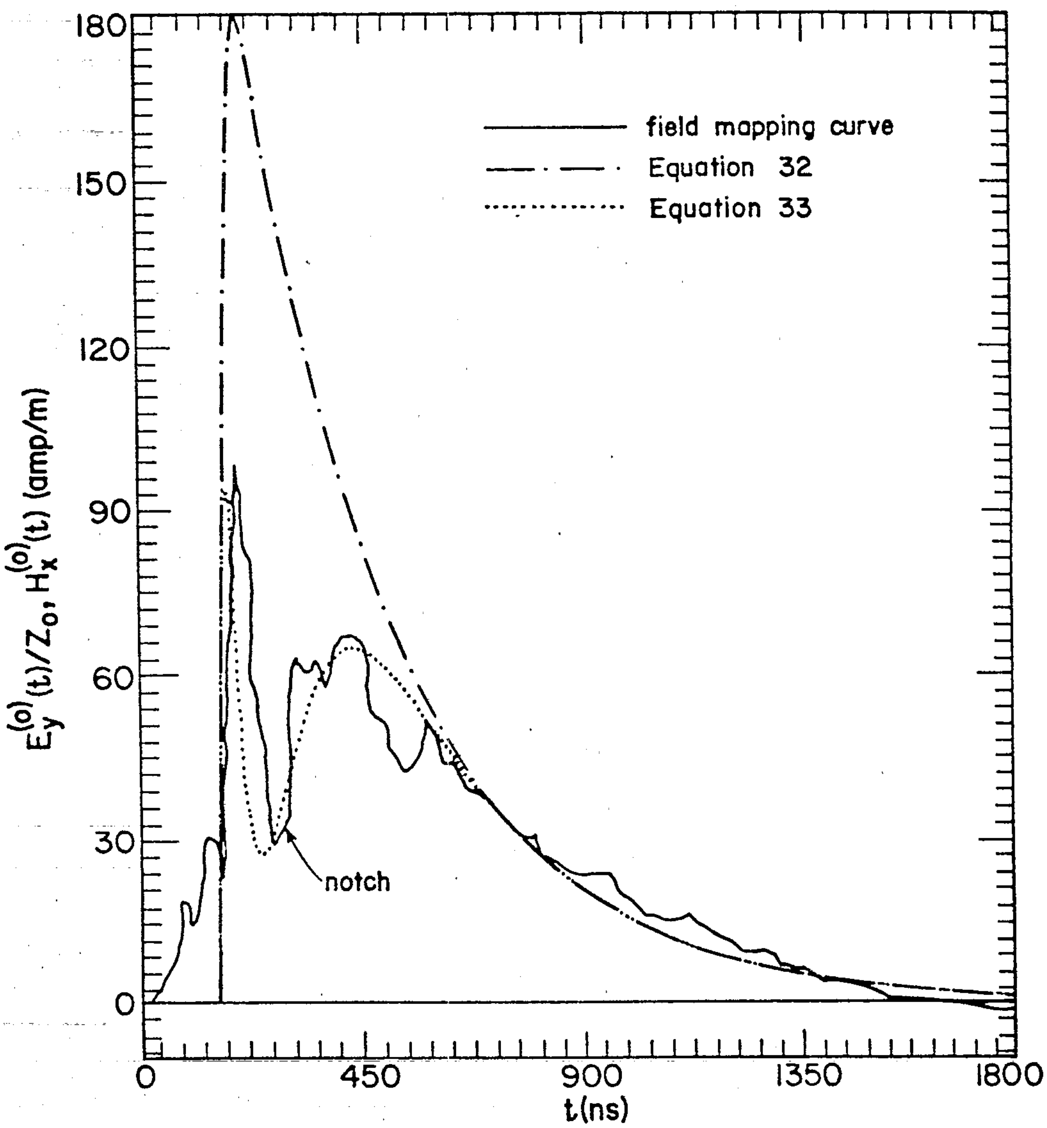

Figure 12. Time-domain curves of $H_x^{(0)}$ and $E_y^{(0)}/Z_o$ at test point 2 from field mapping data (Ref. 11) and analytical representations (Equations 32 and 33).

$$\tilde{H}_z^{(0)}(\omega) = -j\frac{\lambda_o}{\omega\mu_o}\tilde{E}_z^{(0)}(\omega) = j\frac{\lambda_o}{\beta}\tilde{H}_x^{(0)}(\omega)$$

$$\simeq j\frac{\omega(\varepsilon_{1r}-1)a}{2c}\tilde{H}_x^{(0)}(\omega) \qquad (k_o a \ll 1) \tag{34}$$

Thus,

$$H_z^{(0)}(t) \simeq \frac{(\varepsilon_{1r}-1)a}{2c}\frac{\partial}{\partial t}H_x^{(0)}(t)$$

$$= \frac{(\varepsilon_{1r}-1)a}{2c}\frac{\tilde{H}_o}{(t_1-t_2)}\left[\frac{1}{t_1}e^{-t/t_1} - \frac{1}{t_2}e^{-t/t_2} + \frac{1.8}{t_o}\left(1-\frac{t}{t_o}\right)e^{-t/t_o}\right] \tag{35}$$

$$(\text{for } t > t_1)$$

Equation 35 is plotted in Figure 13 where a typical field mapping curve is superimposed. The estimated $H_z^{(0)}(t)$ resembles the field mapping curve, although relatively low in magnitude. The under-estimate of the late-time $H_z^{(0)}(t)$-value is probably due to the following reasons:

1. The sensor used in the field mapping test did not have an accurate response at low frequencies, or, more specifically, gave an over-estimate at the low-frequency region (see Figure 9).
2. The fact that the wood platform is of finite extent is not taken into account in the theory.

A final remark should be made about Equations 32, 33 and 35. They are derived for a field point not too high above the wooden platform. Thus, they are valid only at field points where $\lambda_o x < 1$ for the important spectrum range. From Figure 7, it is observed that $\lambda_o a \simeq 0.06$ for $k_o a \simeq 0.2$ and $\varepsilon_{1r} = 4$. This means that for $a \simeq 1\text{m}$ and frequency $\simeq$ 10 MHz, the decaying distance D, defined by $\lambda_o D = 1$ is approximately given by

$$D \simeq 16.5 \text{ meters} \tag{36}$$

Also, D is proportional to $(\text{frequency})^{-2}$ at lower frequencies. It is therefore reasonable to conclude that Equations 32, 33 and 35 are satisfactory representations for the ATLAS I fields up to as high as 15 meters above the wooden platform.

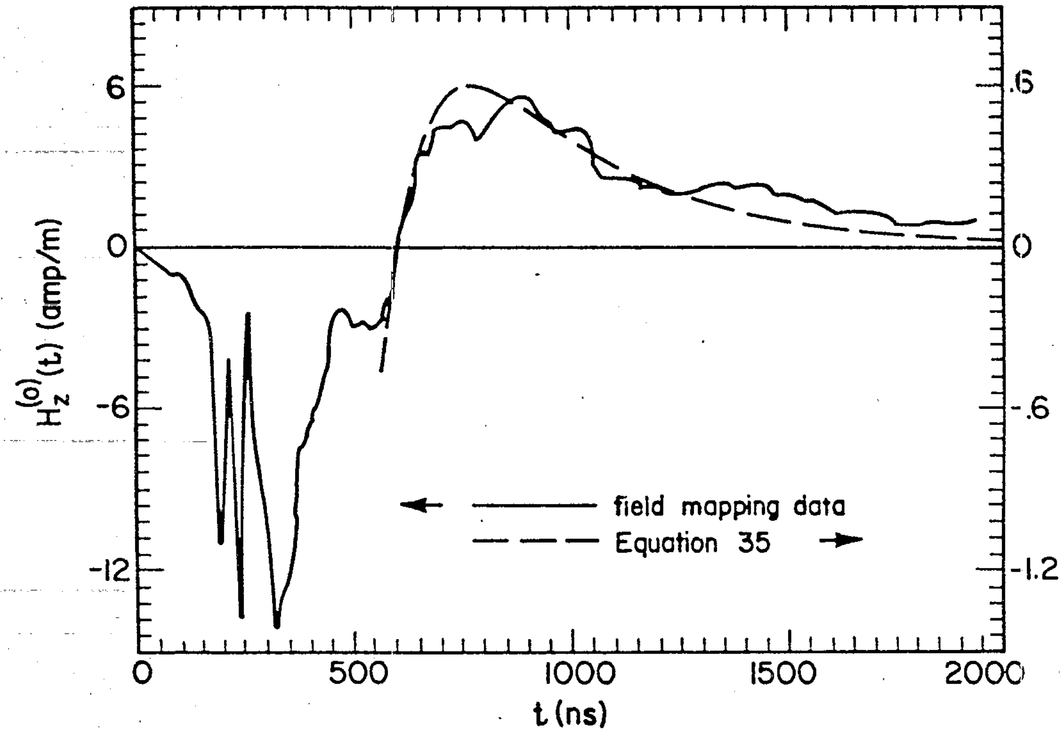

Figure 13. Time-domain curves of $H_z^{(0)}$ at test point 2 (Ref.11) from field mapping data and analytical representation (Equation 35).

Although $\varepsilon_{1r} = 4$ and $a = 1m$ have been selected for the above analysis, other values that show good agreements in Figures 8 and 9 can be used as well (e.g., $\varepsilon_{1r} = 6$, $a = 0.5m$). The reason for selecting $\varepsilon_{1r} = 4$ and $a = 1m$ is that they are closer to the actual situation. However, no matter what values are used, Equations 32, 33 and 35 still hold true while the D-values (i.e., Equation 36) will vary somewhat.

V. SUMMARY

In this report, the following simple analytical expressions have been obtained for the fields above the wood platform of the ATLAS I simulator:

$$E_y^{(0)}(t) = 7.5 \times 10^4 \left(e^{-3.3\times10^6 t} - e^{-1.2\times10^8 t} - 3 \times 10^7 t \; e^{-1.6\times10^7 t} \right) \text{ V/m}$$

$$B_x^{(0)}(t) = 2.5 \times 10^{-4} \left(e^{-3.3\times10^6 t} - e^{-1.2\times10^8 t} - 3 \times 10^7 t \; e^{-1.6\times10^7 t} \right) \text{ webers/m}^2$$

$$B_z^{(0)}(t) = 4.2 \times 10^{-6} \left(e^{-3.3\times10^6 t} - 36 e^{-1.2\times10^8 t} + 9(1 - 1.6\times10^7 t) e^{-1.6\times10^7 t} \right) \text{ webers/m}^2$$

where $B_z^{(0)}(t)$ is valid only for $t > 3 \times 10^{-7}$ sec. These fields can be compared with the "criteria" EMP fields given by (Ref. 13)

$$E(t) = 5.24 \times 10^4 \left(e^{-4 \times 10^6 t} - e^{-5 \times 10^8 t} \right) \text{ V/m}$$

$$B(t) = 1.75 \times 10^{-4} \left(e^{-4 \times 10^6 t} - e^{-5 \times 10^8 t} \right) \text{ webers/m}^2$$

The term that corresponds to the "notch" has a double peak on the negative real axis of the s-plane. This double pole lies between the two single poles that correspond to the double exponentials.

REFERENCES

(1) Baum, C.E., D.V. Giri and R.D. González, "Electromagnetic Field Distribution of the TEM Mode in a Symmetrical Two-Parallel-Plate Transmission Line," Sensor and Simulation Notes, Note 219, Air Force Weapons Laboratory, Kirtland Air Force Base, New Mexico, April 1976.

(2) Marin, L., "Modes on a Finite-Width, Parallel-Plate Simulator: I. Narrow Plates," Sensor and Simulation Notes, Note 201, Air Force Weapons Laboratory, Kirtland Air Force Base, New Mexico, September 1974.

(3) Marin, L., "Modes on a Finite-Width Parallel-Plate Simulator: II. Wide Plates," Sensor and Simulation Notes, Note 223, Air Force Weapons Laboratory, Kirtland Air Force Base, New Mexico, March 1977.

(4) Marin, L., and G.C. Lewis, "Modes on a Finite-Width Parallel-Plate Simulator: III. Numerical Results for Modes on Wide Plates," Sensor and Simulation Notes, Note 227, Air Force Weapons Laboratory, Kirtland Air Force Base, New Mexico, September 1977.

(5) Yang, F.C., "Discrete and Continuous Spectra of Finite-Width, Parallel-Plate Simulator's Fields, "Sensor and Simulation Notes, Note 262, Air Force Weapons Laboratory, Kirtland Air Force Base, New Mexico, June 1979.

(6) Lam, J., "Excitation of the Parallel-Plate Section of a Bounded-Wave EMP Simulator by a Conical Transmission Line," Sensor and Simulation Notes, Note 263, Air Force Weapons Laboratory, Kirtland Air Force Base, New Mexico, May 1979.

(7) Lam, J., "Interaction Between a Parallel-Plate EMP Simulator and a Cylindrical Test Object," Sensor and Simulation Notes, Note 264, Air Force Weapons Laboratory, Kirtland Air Force Base, New Mexico, June 1979.

(8) Wu, T.T., et al., "Experimental Studies on a Scale Model Parallel-Plate Transmission Line Type of EMP Simulator," Miscellaneous Simulator Memos, Memo 18, Air Force Weapons Laboratory, Kirtland Air Force Base, New Mexico, July 1979.

(9) Giri, D.V., et al., "Parallel Plate Transmission Line Type of EMP Simulators: A Systematic Review and Recommendations," Sensor and Simulation Notes, Note 261, Air Force Weapons Laboratory, Kirtland Air Force Base, New Mexico, April 1980.

(10) Varvatsis, A.D., S.G. Siegel, and M.I. Sancer, "Numerical Investigation of Plane Wave Pulse Scattering by Dielectric Obstacles/Detailed Results for a Dielectric Slab Model of the ATLAS I TRESTLE Platform," Sensor and Simulation Notes, Note 233, Air Force Weapons Laboratory, Kirtland Air Force Base, New Mexico, October 1977.

(11) Merewether, D.E., et al., "Field Mapping Data for ATLAS I: Vol. I-IV," ATLAS Memos, Memo 27-30, Air Force Weapons Laboratory, Kirtland Air Force Base, New Mexico, January 1980.

(12) Latham, R.W., "Reflection from an Array of Dielectric Posts," Sensor and Simulation Notes, Note 180, Air Force Weapons Laboratory, Kirtland Air Force Base, New Mexico, June 1973.

(13) Castillo, J.P., "An Estimate of the Open-Circuit Voltages Induced in a Loop Due to an Incident EMP," Interaction Application Memos, Memo 1, Air Force Weapons Laboratory, Kirtland Air Force Base, New Mexico, December 1973.